LA-UR-21-27018
Approved for public release; distribution is unlimited.

Title: Simulation of the PBX 9501 Self-Ignited Heavily Confined Cookoff Test

Author(s): Aviles-Ramos, Cuauhtemoc

Intended for: Report

Issued: 2021-07-20

Simulation of the PBX 9501 Self-Ignited Heavily Confined Cookoff Test

Aviles-Ramos, Cuauhtemoc

Advanced Engineering Analysis, W-13
Los Alamos National Laboratory
Los Alamos New Mexico 87545

Abstract

The PBX 9501 self-ignited thermally damaged explosive (SITX) test was carried out by Holmes et al. [1]. A 6-inch diameter sphere made of the PBX 9501 was heated inside a steel confinement vessel until it underwent a thermal explosion. This test provided measured temperature data that was used to define a boundary condition to carry out post-experiment finite element (FE) thermal simulations and comparisons of the FE thermal response with the experimental time to thermal ignition and internal temperature measurements at the center of the PBX 9501 sphere. Finite element models of this experiment were constructed using the heat transfer code Aria [2]. A cookoff model for PBX 9501 [3] was used to simulate the thermal decomposition of PBX 9501 and to predict the time to thermal ignition. An inverse heat conduction scheme was designed and applied to estimate a 1D temperature boundary condition.
Keywords: Ignition kinetics, Thermal runaway, Non-linear heat conduction.

Heavily Confined SITX Test Description and Observations

This test was intended to have a sealed configuration. Figure 1 shows a sketch of the test. The SITX test contained a sphere of PBX 9501 with a mass of 3.407 kg. The assembly

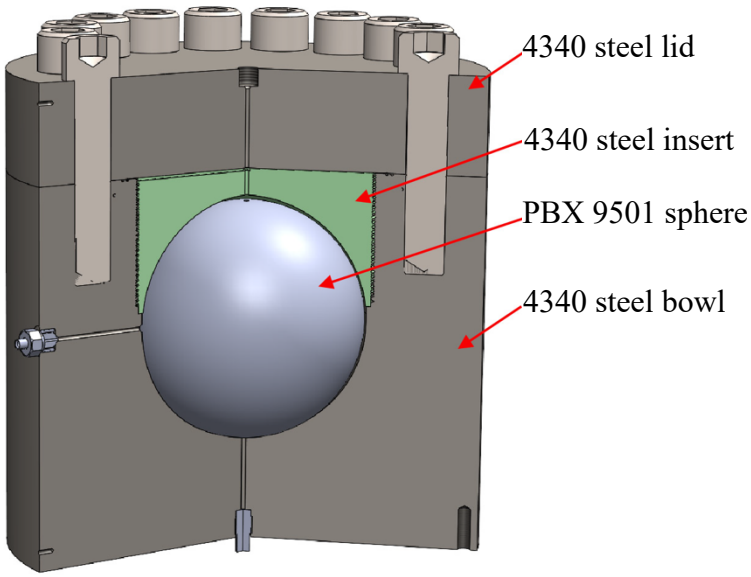

Figure 1. Sketch of sphere in steel vessel.

was wrapped around with heating tape. Temperatures inside the explosive were measured through a blind hole drilled on top of the sphere. Thermocouples type K were potted into this hole at different heights. Figure 2 shows the locations of these thermocouples and Figure 3 shows the

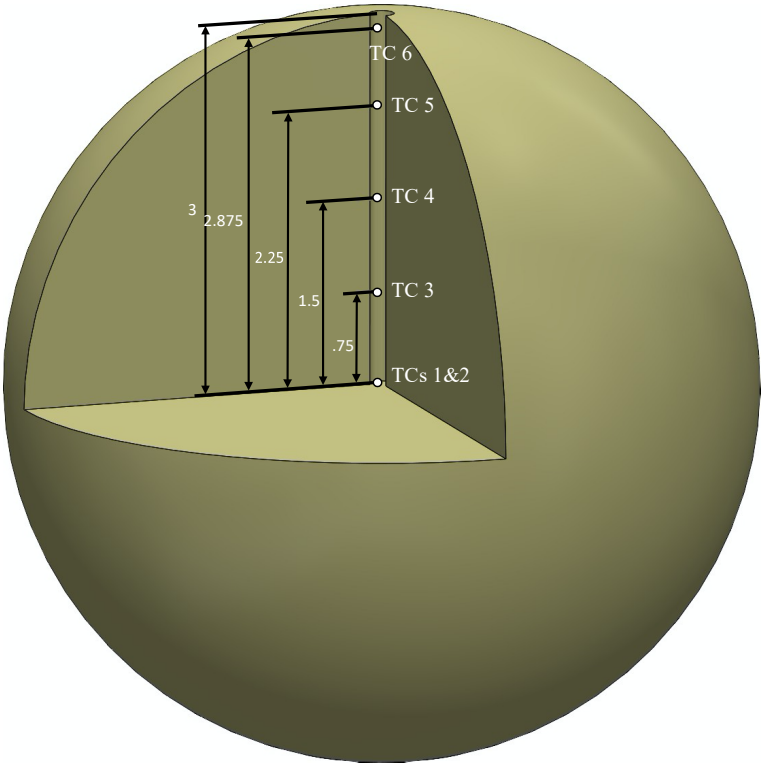

Figure 2. Thermocouples potted inside a hole on the PBX 9501 sphere.

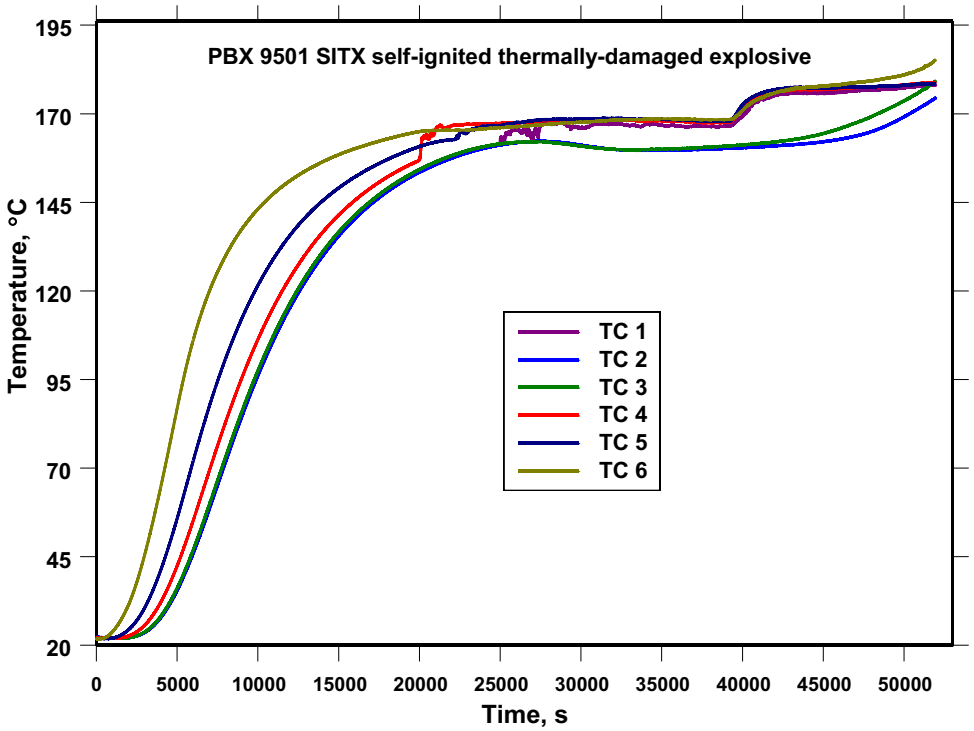

Figure 3. Internal temperatures measured by TCs shown in Figure 2.

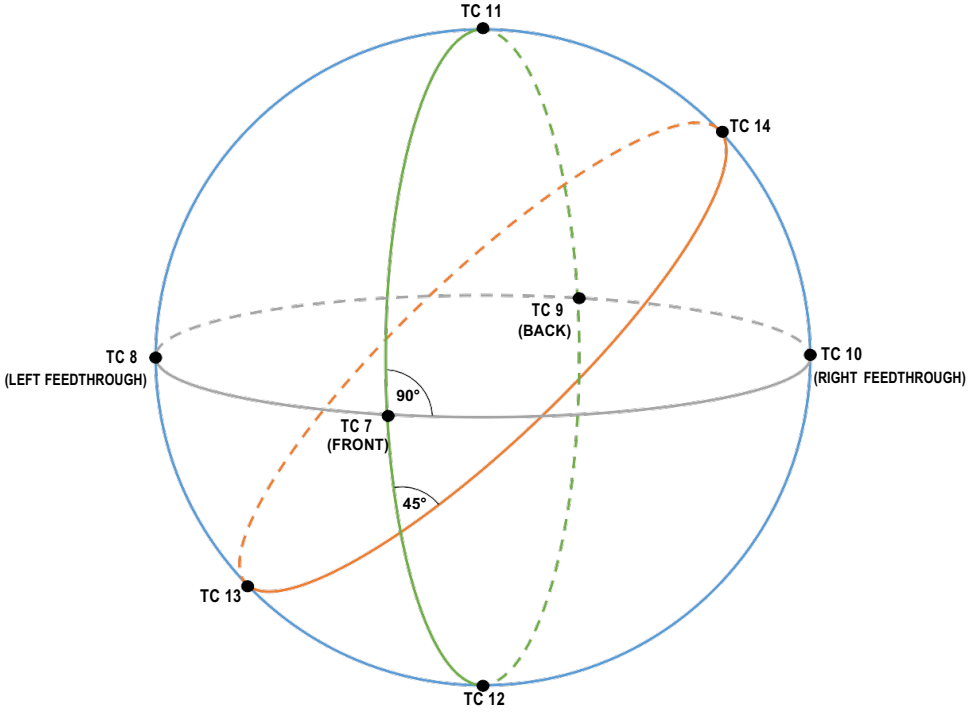

Figure 4. Thermocouples installed on the surface of the PBX 9501 sphere.

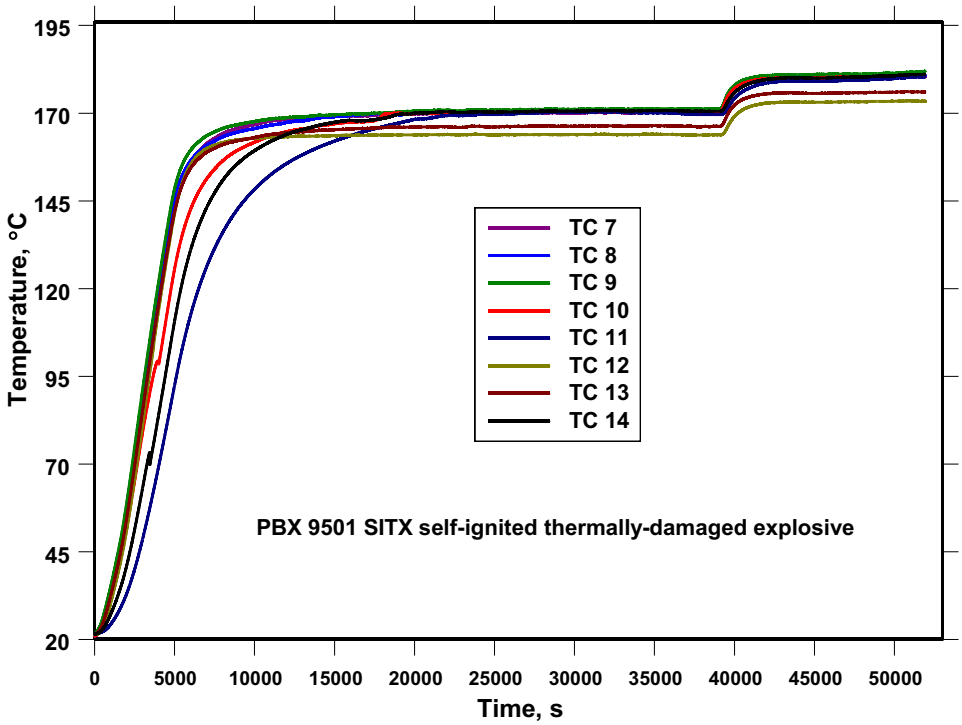

Figure 5. Temperature measured by the thermocouples shown in Fig. 4.

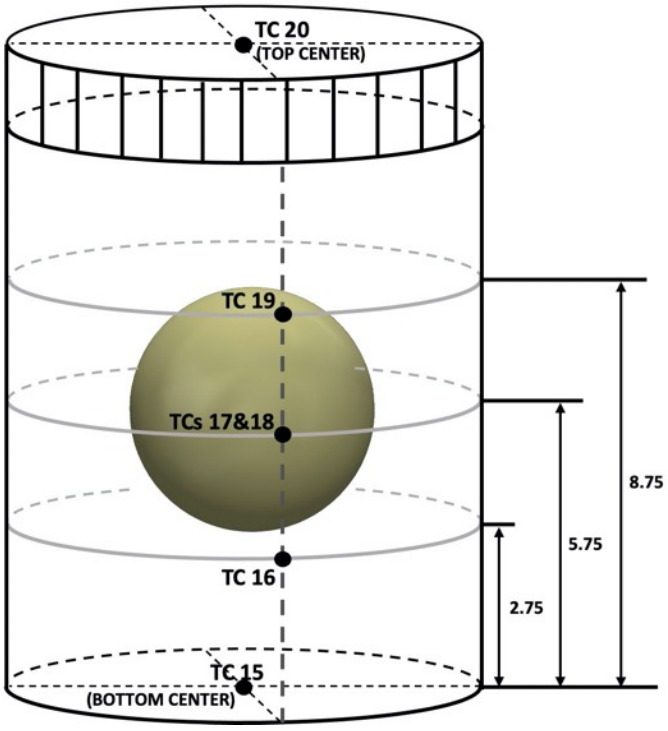

Figure 6. Thermocouples installed on outer surface of the confinement vessel.

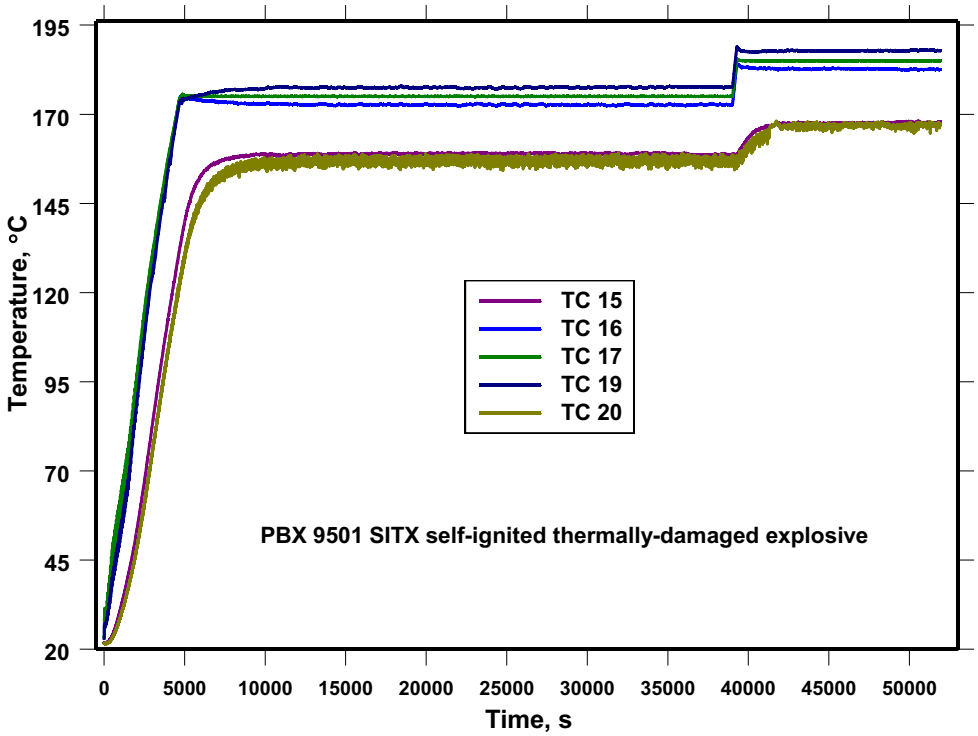

Figure 7. Temperatures measured by the TCs shown in Figure 6.

the measured temperatures at the locations shown in Fig. 2. Eight thermocouples were installed on the surface of the sphere. Figure 4 shows the location of these thermocouples and Fig. 5 shows the tempereatures measured by the thermocouples shown in Fig. 4. There were six thermocouples installed on the outer surface of the confinement vessel. Figure 6 shows the location of these external thermocouples and Fig. 7 shows the temperatures measured by the thermocouples shown in Fig. 6. The simulations carried out in this report used the temperatures measured by the thermocouples installed on the spherical surface shown in Fig. 4.

The experimental thermal ignition was achieved at 14.4272 hours (51938 s) after the heating was started. The temperature thermal runaway in the explosive was not detected by the internal thermocouples because thermal ignition took place at a different location than the positions of the thermocouple shown in Fig. 2. A thermal decomposition model for PBX 9501 developed by Dickson, et al. [4] and parameterized by Aviles-Ramos [3] was used to model this experiment using temperature boundary conditions defined on the surface of the sphere. This model is described in the next section.

PBX 9501 Cookoff Model

A parameterization of the Dickson et al. model [3] was implemented in Aria [2]. The Dickson et al. mechanism [4] considers 4 steps

1. HMX (β) $\leftrightarrow$ HMX (δ)
   (first order endothermic)
2. HMX (β) + HMX (δ) $\leftrightarrow$ HMX (δ)
   (bimolecular endothermic)
3. HMX (δ) $\rightarrow$ *products*
   (1st order endothermic)
4. HMX (δ) + *products* $\rightarrow$ *products*
   (bimolecular exothermic)

The reaction rates associated with steps 1, 2, 3, and 4 are

$$\Re_1 = k_{1f} M_a - k_{1r} M_b \tag{1}$$

$$\Re_2 = M_a M_b \left(k_{2f} - k_{2r}\right) \tag{2}$$

$$\Re_3 = k_3 M_b \tag{3}$$

$$\Re_4 = k_4 M_b M_c \tag{4}$$

The rate constants are defined by

$$k_{1f} = \frac{k_B T}{h} \exp\left[\frac{T\Delta S_{1f} - E_{1f}}{RT}\right] \tag{5}$$

$$k_{1r} = \frac{k_B T}{h} \exp\left[\frac{T\Delta S_{1r} - E_{1r}}{RT}\right] \tag{6}$$

$$k_{2f} = \frac{k_B T}{h} \exp\left[\frac{T\Delta S_{2f} - E_{2f}}{RT}\right] \tag{7}$$

$$k_{2r} = \frac{k_B T}{h} \exp\left[\frac{T\Delta S_{2r} - E_{2r}}{RT}\right] \tag{8}$$

$$k_3 = Z_3 \exp\left(\frac{-E_3}{RT}\right) \tag{9}$$

$$k_4 = \begin{cases} 8.0\times10^{15} \exp\left(\dfrac{-1.69090\times10^5}{R\,T}\right) \text{ for } T \le 453.15\ \text{K} \\ 5.082\times10^{10} \exp\left(\dfrac{-14916.2}{T} - 7.0516\times10^{-7}T \right. \\ \qquad \left. + 6.4899\times10^{-4}\ln T\right) \text{ for } 453.15\ \text{K} < T < 466.15\ \text{K} \\ 8.0\times10^{15} \exp\left(\dfrac{-1.70383\times10^5}{R\,T}\right) \text{ for } T \ge 466.15\ \text{K} \end{cases} \tag{10}$$

The variables M_a, M_b, and M_c are the mass fractions of β–HMX, δ–HMX, and gas products respectively. The rate k_4 given by Eq. (10) is the main modification of the original Dickson et al. kinetics model [4]. The parameters used to define Eq. (10) were estimated [3] using 13 Sandia Instrumented Thermal Ignition (SITI) experiments that involved the cookoff of PBX 9501 cylinders. The old definition of k_4 in the original model [4] was: $Z_4 \exp(-E_4/RT)$ where the activation energy E_4 was a constant. The kinetic parameters are given in Table 1. The system of partial differential equations that represent this kinetics were obtained assuming that mass is conserved

Table 1. Kinetic parameters for Eq. (1)–(9). The symbols k_B and h are Boltzman's and Plank's constants respectively.

$k_i(T)$	Z_i, 1/s	ΔS_{if}, J/mol K	E_{if}, J/mol	ΔS_{ir}, J/mol K	E_{ir}, J/mol
k_{1f}		123	2.040×10^5		
k_{1r}				89.0	1.890×10^5
k_{2f}		–40.37	1.015×10^5		
k_{2r}				–75.2	8.650×10^4
k_3	3.16×10^{16}		2.000×10^5		

$$\frac{\partial M_a}{\partial t} = -\Re_1 - \Re_2 \tag{11}$$

$$\frac{\partial M_b}{\partial t} = \Re_1 + \Re_2 - \Re_3 - \Re_4 \tag{12}$$

$$\frac{\partial M_c}{\partial t} = \Re_3 + \Re_4 \tag{13}$$

This ignition kinetics is assumed to be coupled to the heat conduction equation in the PBX 9501 through the definition of a volumetric heat generation term

$$Q(T) = \rho_0 \sum_{j=1}^{4} \Delta H_j \Re_j \tag{14}$$

where ΔH_1= –52 kJ/kg, ΔH_2 = –52 kJ/kg, ΔH_3= –120 kJ/kg, and ΔH_4= 3200 kJ/kg are the heats of reaction for each step. The energy equation in the PBX 9501 for the LSAC experiments is taken as

$$\nabla \cdot \left(\kappa_{avg} \nabla T\right) + Q = \rho_0 C^*_{avg} \frac{\partial T}{\partial t} \tag{15}$$

where ρ_0 = 1.849 g/cm^3 is the bulk density, Q is the energy generation term defined by Eq. (14), and the average thermal properties are calculated using the mass fractions as weighting coefficients

$$\kappa_{avg} = M_a \kappa_\beta + M_b \kappa_\delta + M_c \kappa_{products} \tag{16}$$

$$C^*_{avg} = M_a C^*_\beta + M_b C^*_\delta + M_c C^*_{products} \tag{17}$$

$$\kappa_n = \kappa_1^n + \kappa_2^n T \tag{18}$$

$$C^*_n = C_1^{*n} + C_2^{*n} T \tag{19}$$

where n = δ, β, and *products*. The parameters associated with Eqs. (18) and (19) are given in Table 2.

Table 2. Parameters in Eqs. (40) and (41).

n	C_1^{*n} J/kg K	C_2^{*n} J/kg K^2	κ_1^n W/m K	κ_2^n W/m K^2
β	236	2.7	0.75	-9.5×10^{-4}
δ	236	2.7	0.53	-5.4×10^{-4}
products	222	2.45	2.0	0.00

The cookoff model defined by Eqs. (1) to (19) is not pressure dependent. However, an average pressure at each FE time step can be calculated using an equation of state. The reacted solid fraction is calculated first

$$S_f = M_a + M_b \tag{20}$$

The gas volume fraction is obtained using the solid fraction from Eq. (20) as

$$\phi = 1 - \frac{\rho_{c,0}\, S_f\, (1 - \phi_0)}{\rho_c} \tag{21}$$

where $\rho_{c,0} = 1860$ kg/m^3 is the initial condensed density, ϕ_0 is the initial gas volume fraction, and ρ_c is the condensed density which is assumed to vary with temperature according to [5]

$$\rho_c = \begin{cases} \rho_{c,o}\left[1 - 0.000131\left(T - T_0\right)\right], \text{ when } T \le 444 \text{ K} \\ \rho_{c,o}\left\{\left[1 - 0.000131\left(T - T_0\right)\right] - 0.067\right\}, \text{ when } T > 444 \text{ K} \end{cases} \tag{22}$$

where T_0 is the initial temperature. The calculations done in this report assume that the variation of ρ_c with temperature is limited by the value of the bulk density, $\rho_0 = 1849$ kg/m^3. Note from Eq. (22) that ρ_c decreases as the temperature increases. Once ρ_c reaches a value of 1849 kg/m^3, it is kept constant equal to the bulk density. The initial gas volume fraction is calculated from

$$\phi_0 = \frac{\rho_{c,0} - \rho_0}{\rho_{c,0} - \rho_{gas,0}} \tag{23}$$

where ρ_{gas} is calculated from the ideal gas law

$$\rho_{gas,0} = \frac{P_0}{R\, T_0} \tag{24}$$

The gas volume is calculated integrating Eq. (21) over the PBX 9501 volume

$$V_g = \int_V \phi \, dV \tag{25}$$

The PBX 9501 average temperature and the number of moles are calculated as

$$T_{ave} = \frac{\int_V T \, dV}{\int_V dV} \tag{26}$$

$$n = \int_V \frac{\rho_0 \; M_c}{M_{w,\, products}} \, dV \tag{27}$$

where $M_{w,\, products}$ is the average molecular weight of the products (40 kg/kg mol) which are a mixture of the thermal decomposition gases produced in steps 3. and 4. of the decomposition mechanism. The ideal gas equation of state can be used to calculate pressure using Eqs. (25), (26), and (27). For the case of non-ideal gas behavior, the Becker-Kistiakowsky-Wilson (BKW) was used [5].

$$P = \frac{n\, R\, T_{ave}}{V_g} \tag{28}$$

The cookoff model defined by Eqs. (1) to (19) was implemented in Aria [2]. User subroutines were written in C to implement the calculation of the thermal conductivity and the heat capacity. Also, C user subroutines were written to implement the reaction rates and the source term defined by Eq. (14).

Temperature Boundary Conditions and Simulations of the SITX Experiment

As a first attempt to model this experiment, all the thermcouples shown in Fig. 4 were used to define 3D boundary condition on the surface of the sphere. The definition of this boundary condition was done using a C/C++ user plug-in available in the FE code Aria [2]. This user subroutine makes available the Cartesian coordinates of the nodes that define the finite element faces on the outer surface of the PBX 9502 sphere. These coordinates are transformed into spherical using the coordinate system depicted in Figure 8. This user subroutine makes available the Cartesian coordinates of the nodes

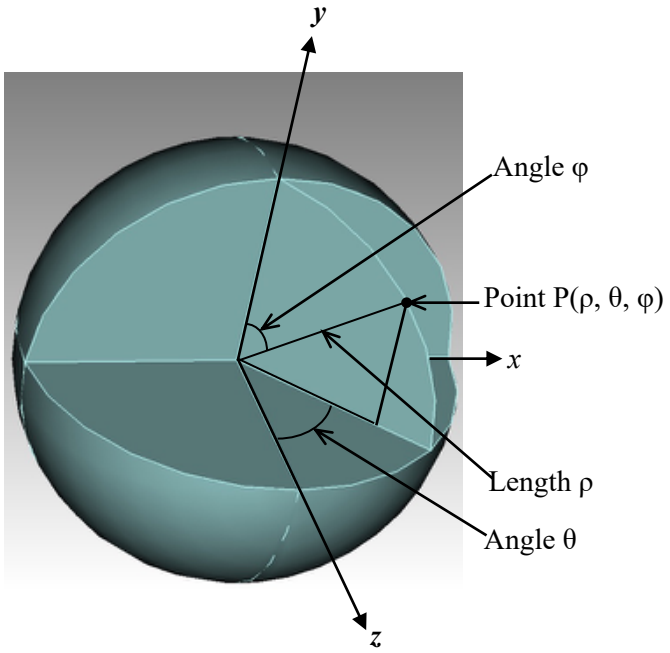

Figure 8. Coordinate system used to calculate the spherical coordinates of the nodes located on the outer surface of the PBX 9501 sphere.

that define the finite element faces on the outer surface of the PBX 9501 sphere. These coordinates are transformed into spherical using the coordinate system depicted in Fig. 8.

The temperature on the nodes located between the thermocouples shown in Fig. 4 was calculated assuming the surface temperature is a linear function of the angles θ and φ. Four interpolation schemes were implemented to calculate the nodal surface coordinates on and between the meridians located on the (z, y), $(z, -y)$, (x, y), $(x, -y)$, $(-z, y)$, $(-z, -y)$, $(-x, y)$, and $(-x, -y)$ planes. These schemes were implemented in four user subroutines written in C made available in Aria [2]. The relationships between the spherical and rectangular coordinate systems shown in Fig. 8 used to calculate the angular coordinates of the nodes of the FE mesh on the surface of the PBX 9502 sphere are

$$x = \rho \sin(\varphi)\sin(\theta),\ y = \rho \cos(\varphi),\ z = \rho \sin(\varphi)\cos(\theta) \tag{29}$$

$$\theta = \arctan\left(\frac{x}{z}\right) = \arccos\left(\frac{z}{\sqrt{z^2 + x^2}}\right) = \arcsin\left(\frac{x}{\sqrt{z^2 + x^2}}\right) \tag{30}$$

$$\varphi = \arctan\left(\frac{\sqrt{z^2 + x^2}}{y}\right) = \arccos\left(\frac{y}{\sqrt{z^2 + x^2 + y^2}}\right) \tag{31}$$

for $\rho \geq 0$, $0 \leq \theta \leq 2\pi$, and $0 \leq \phi \leq \pi$.

A three dimensional mesh of the PBX 9501 sphere was constructed. This mesh, the user subroutines that were constructed to implement a 3D boundary condition on the surface of the sphere, and the user subroutines constructed to implement the PBX 9501 cookoff model described in the previous section were used to carry out the first simulation of the SITX experiment. It was decided to use all the thermocouples shown in Fig. 4 to see if a reasonable prediction of the time to thermal ignition could be obtained. Figure 9 shows a comparison of the FE model response at the center of the sphere with TC 2 shown in Fig. 2 is given in Figure 9. This figure shows that the

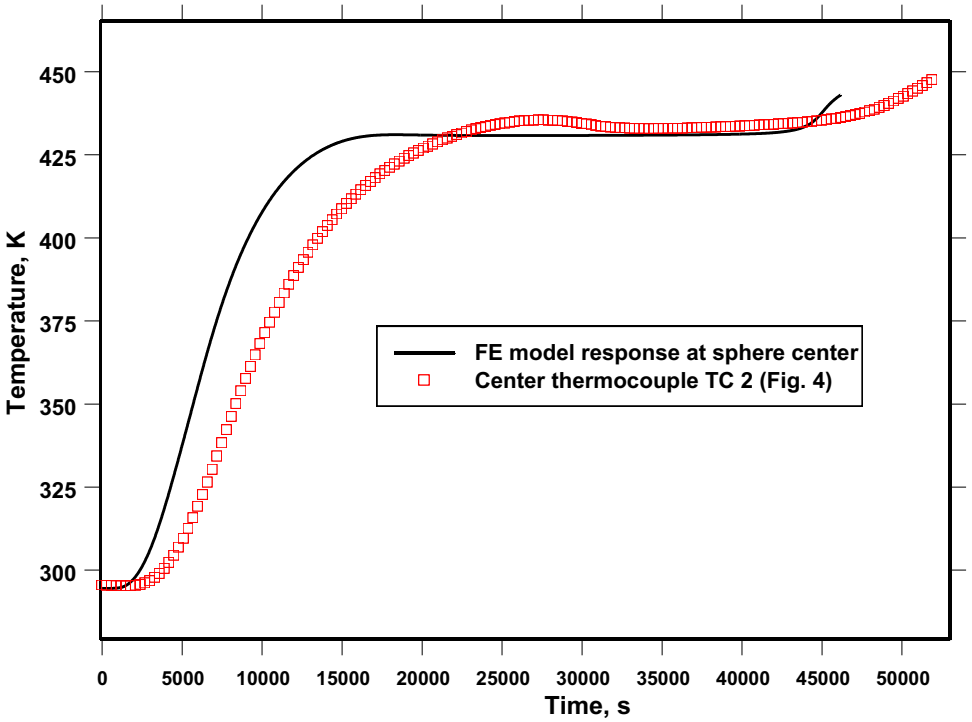

Figure 9. Comparison of the calculated temperature at the center of the sphere with the readings of thermocouple 2.

temperatures calculated by the FE model are significantly larger than the readings of TC 2 for times between zero and 20800 s. The experimental and predicted times to thermal ignition were 51938 s and 46167 s respectively. This produced a time to ignition error of -11%. One of the reasons for the disagreement between the predicted and experimental temperatures is that thermocouples 7, 8, 9, 10, 12, and 13 were taped on the metal bowl. Figures 10 and 11 show these TCs taped to the metal bowl and Figure 12 shows TCs 11 and 14 taped on the surface of the sphere.

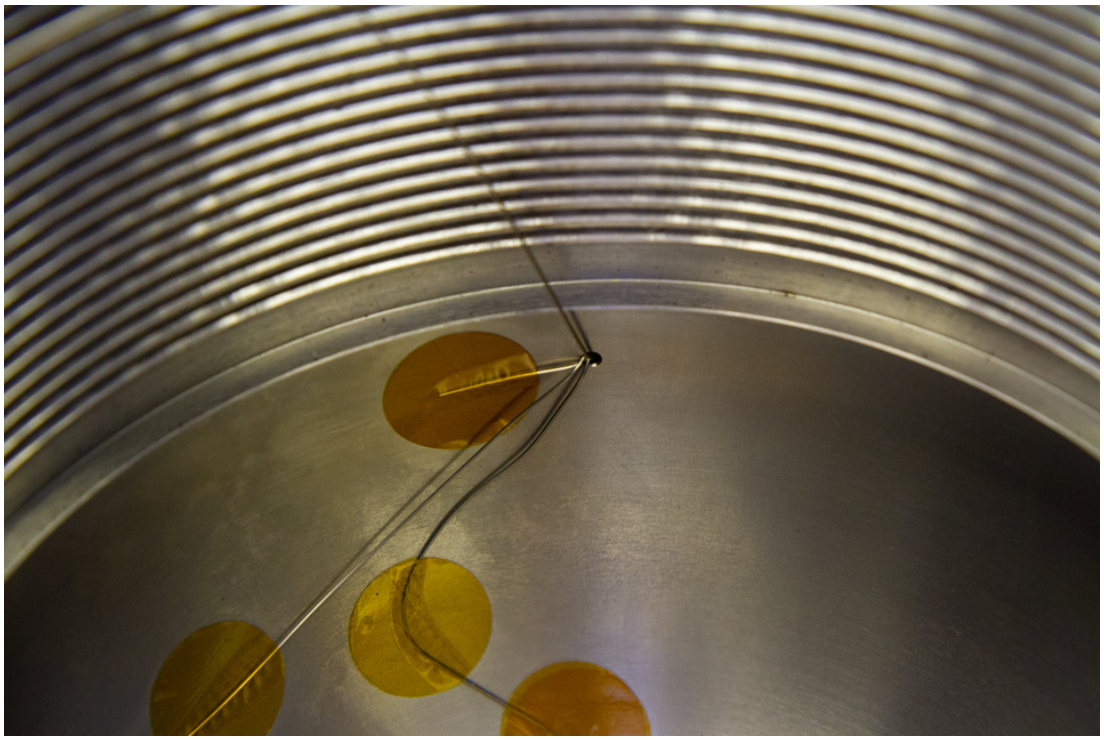

Figure 10. One of the equatorial thermocouples taped to the metal bowl.

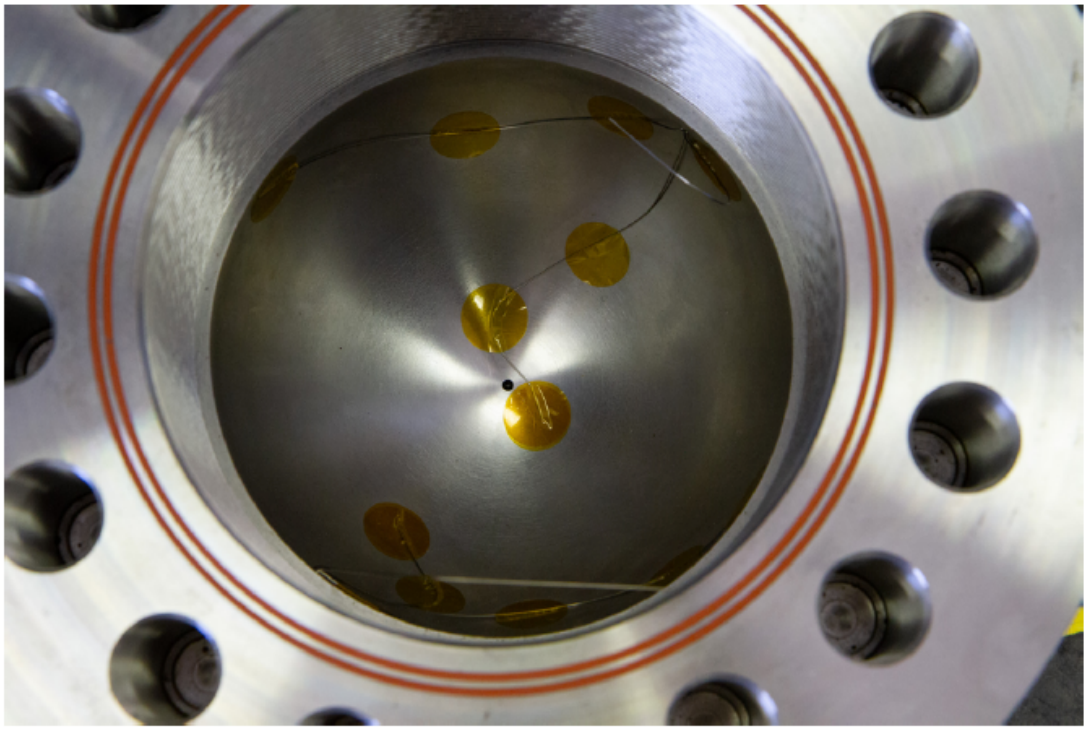

Figure 11. Thermocouples 7, 8, 9, 10, 12, and 13 shown in Fig. 4 taped to the metal bowl.

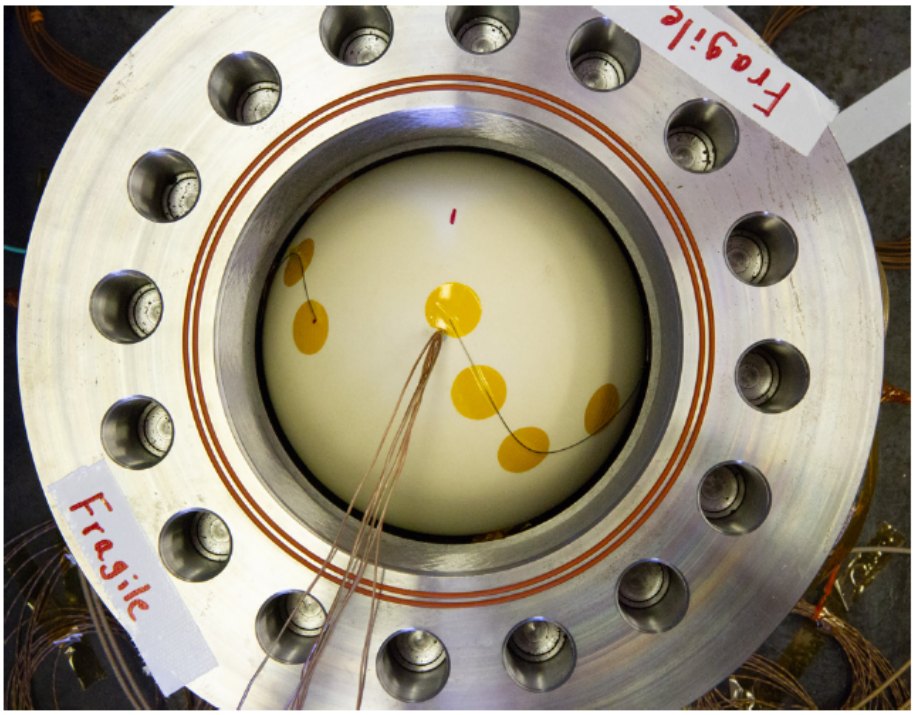

Figure 12. Thermocouples 11 and 14 taped to the top surface of the sphere.

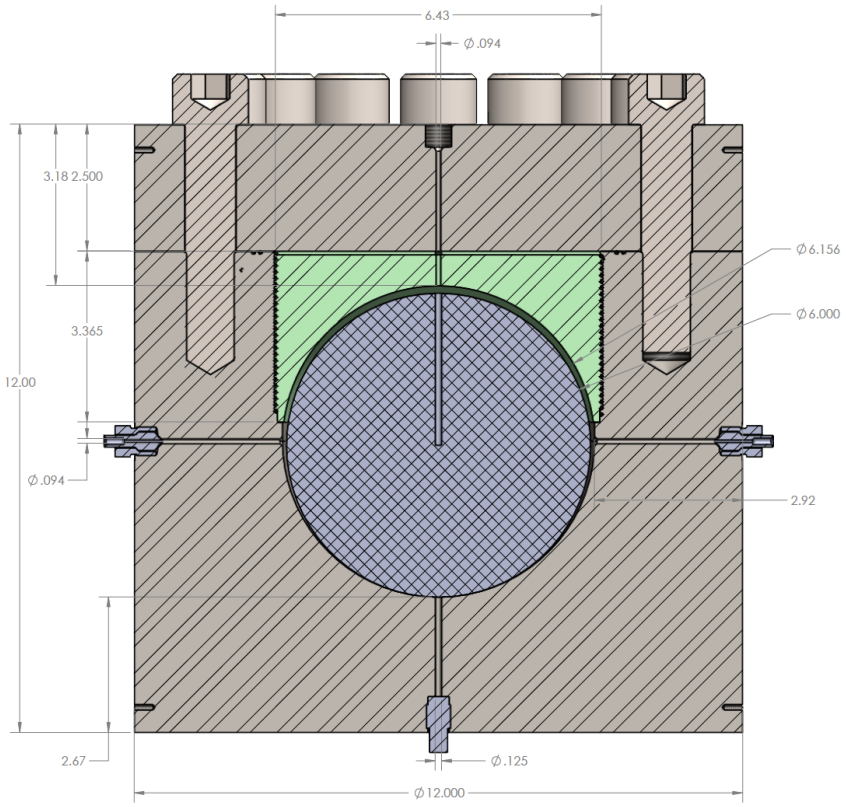

Figure 13. View of the metal confinement and PBX 9501 sphere.

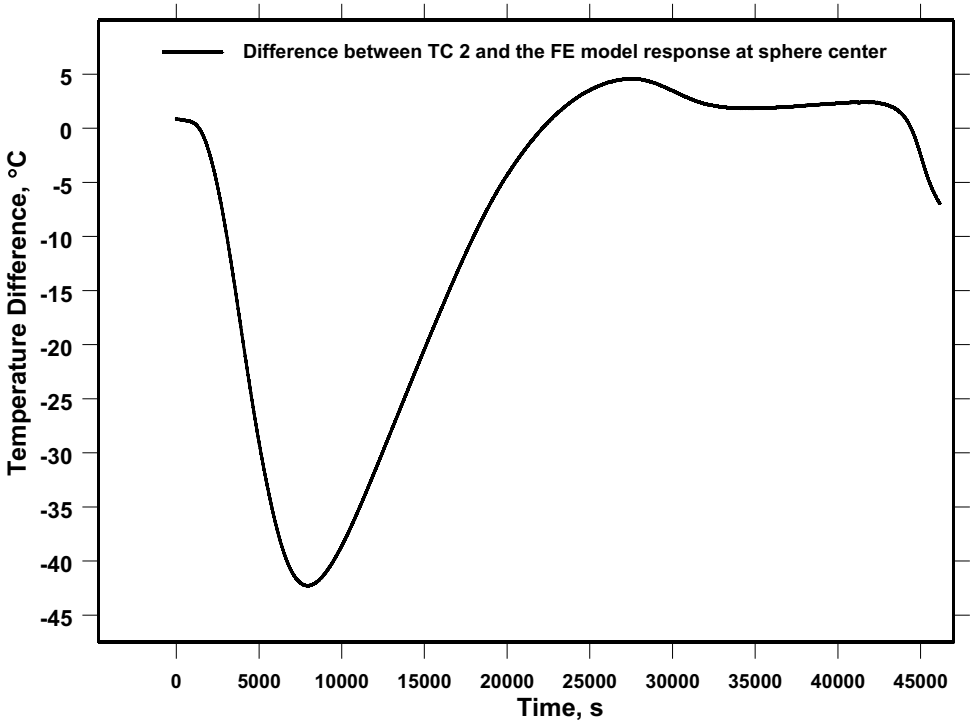

Figure 14. Difference between thermocouple 2 and FE model response at the center of the PBX 9501sphere. This FE solution uses a 3D boundary condition implemented on the surface of the sphere using all the thermocouple readings.

The inner spherical cavity of the metal confinement vessel had a diameter of 6.156 in and the PBX 9501 sphere had a 6 in diameter. This differenence left a 0.078 in (~2 mm) gap filled with air between the metal bowl and the PBX 9501. This gap was not uniform and became smaller on the bottom part of the spherical cavity. Figure 13 shows that this gap is larger on the top surface of the sphere and decreases in the direction of the bottom pole of the sphere. The effect of this gap became smaller as the PBX 9501expanded while it was being heated. The main effect of this air gap was to make the temperatures measured by TCs 7, 8, 9, 10, 12, and 13 larger than the temperatures on the bottom surface of the sphere because of the thermal contact resistance generated by this gap. The main reason for the disagreement between the predicted and experimental temperatures at the center of the sphere shown in Fig. 9 are due to this effect. Thermocouples 11 and 14 were the only thermocouples that were taped on the surface of the PBX 9501 sphere and are likely to be a better representation of the sphere's surface temperatures. Figure 14 shows the difference between thermocouple 2 (center thermocouple) and the FE model response at the sphere center. Figure 14 shows that the temperature differences are significant in the interval $0 \leq t \leq 17500$ s. The main reason for these differences is that the temperature boundary conditions applied at the locations of TCs 7, 8, 9, 10, 12, and 13 are larger than the actual temperatures experienced by the bottom surface of the sphere because they were taped to the steel.

Figure 5 shows that there is close agreement between thermocouples 7, 8, 9, 10, 11, and 14 for times greater than 23000 s. Note that this agreement includes thermocouple 11 and 14 which were the only TCs taped on the surface of the PBX 9501. This agreement is an indication that the experiment was close to one dimensional with respect to the boundary conditions. For fhis reason,

a 1D solution was implemented solving an inverse heat conduction problem to obtain the 1D boundary temperature on the sphere for times smaller or equal to 20800 s. This inverse problem was solved to reduce the large differences in temperature shown in Fig. 14 obtained when a 3D boundary condition that uses all the thermocouple readings was implemented. Thermocouple 2 which was installed at the center of the sphere was used to carry out the inverse estimation of the 1D boundary temperature for $t \leq 20800$ s. The first iteration step in this inverse scheme consists of using the readings of thermocouple 11 as a first guess for the 1D boundary condition on the surface of the sphere and run the FE model with this surface temperature as a boundary condition. This first iteration produces the finite element model predicted temperatures, T_{FE}^1, at the center of the sphere. The second iteration consists of a correction of the first guess of the surface temperature calculated by Eq. (32) as

$$T_s^2 = \frac{T_2}{T_{FE}^1} T_s^1 \tag{32}$$

where T_s^1 represents the readings of thermocouple 11 used as a first guess in the first simulation, T_2 represents the readings of thermocouple 2 at the center of the sphere, and T_s^2 is the corrected surface temperature calculated by Eq. (32) which will be applied as a boundary condition for the second simulation step. The superscript 1 in T_s^1 is used to imply that it is the first guess for the surface temperature of the sphere and the superscript 1 in T_{FE}^1 is used to imply the temperature calculated at the center of the sphere using the FE model with the first guess of the temperature boundary condition. The FE model is ran again to simulate the experiment using the surface temperature T_s^2 calculated by Eq. (32) as a boundary condition. This simulation produces a prediction of the temperature at the center of the sphere, T_{FE}^2. The third iteration consists of a correction of the surface temperature calculated by Eq. (33). The FE model is run again to simulate

$$T_s^3 = \frac{T_2}{T_{FE}^2} T_s^2 \tag{33}$$

the experiment using the surface temperature T_s^3 calculated by Eq. (33) as a boundary condition. This simulation produces a prediction of the temperature at the center of the sphere given by T_{FE}^3. This process is repeated until the predicted temperature at the center of the sphere is in reasonable agreement with the readings of thermocouple 2. The sequential application of Eqs. (32) and (33) can be written as

$$T_s^j = \frac{T_2}{T_{FE}^{j-1}} T_s^{j-1} \tag{34}$$

where $j = 2, 3, \ldots, N$, and N is the number of iterations. Equation (34) reduces to Eqs. (32) and (33) for $j = 2$ and $j = 3$ respectively. The iteration for $j = 5$ in Eq. (34) produced a reasonable agreement between the measured and calculated temperatures at the center of the sphere, T_{FE}^5. The iteration for $j = 5$ was carried out for $t \leq 20800$ s. Thermocouple 11 was selected as a reasonable estimate for the surface temperatures for $t > 20800$ s. Figure 15 shows a graph of the error calculated as Measured – Predicted at the center of the PBX 9501 sphere for $t \leq 20800$ s. Figure

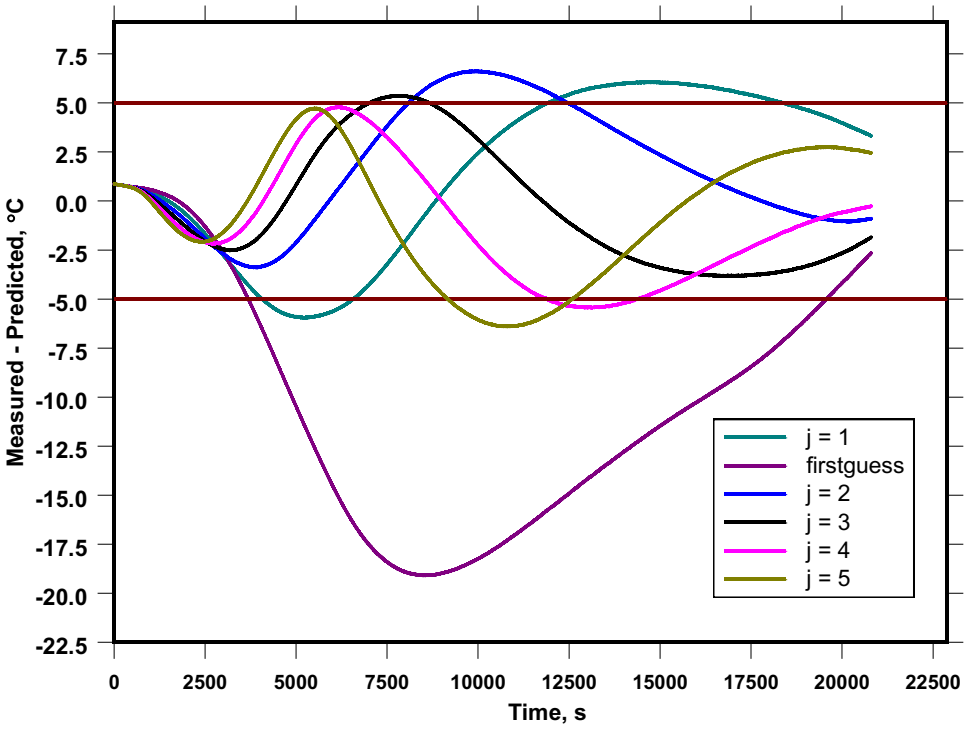

Figure 15. Error between the measured and predicted temperature at the center of the sphere calculated from the sequential application of Eq. (34).

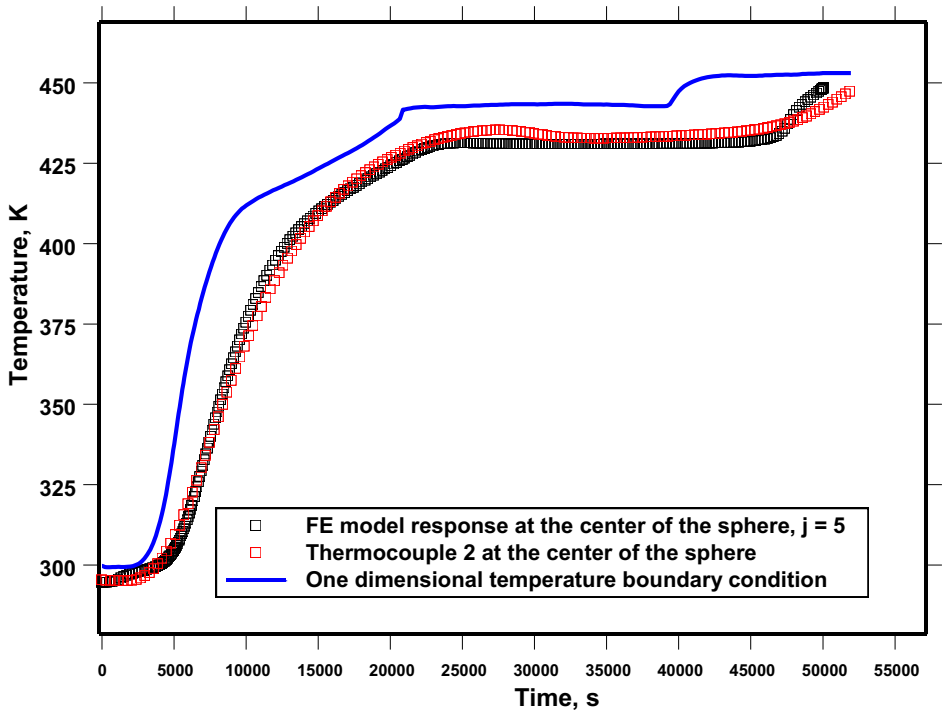

Figure 16. Predicted and experimental temperatures at the center of the PBX 9501 sphere.

15 shows a periodic variation of the error. For this reason, the standard deviation between the measured and calculated temperatures was calculated for the iteration result $j = 5$ using the equation

$$S = \sqrt{\frac{\sum_{i=1}^{M}\left(T_{2,i} - T_{FE,i}^{5}\right)^{2}}{M-1}} \tag{35}$$

where M is the number of temperature measurements for $t \leq 20800$ s. The calculated value of S was 3.3 °C. This value is considered to be reasonable taking into consideration that the thermocouples used were of type K with a measurement accuracy of ±2.2 °C. Figure 16 compares the calculated temperatures at the center of the PBX 9501 sphere, T_{FE}^{5}, with the temperatures measured by thermocouple 2. The estimated surface temperature is also shown in Fig. 16. The simulation that produced the results shown in Fig. 16 predicted the time to thermal ignition at 50072 s. The experimental time to thermal ignition was 51938 s. This results in a percentage error of -3.6%.

Equation (35) was used to calculate a value of S of 3.3 °C between the measured and calculated temperatures at the center of the sphere for $t \leq 20800$ s. This reassures that the 1D boundary condition that was applied on the surface of the sphere for $t \leq 20800$ s is realistic. A more realistic axisymmetric boundary condition can be implemented for $t > 20800$ s. The implementation of this boundary condition is possible because the readings of thermocouples 7, 8, 9, and 10 vary within a temperature interval with a width of 2.3 °C. Figure 17 shows the width of this interval. Note that for the most part, the readings of the equatorial thermocouples 7, 8, 9, and 10 are within the interval: 179.93 °C $\leq T \leq$ 181.24 °C. This means that it is possible to consider that the average of thermocouples 7, 8, 9, and 10 can be used to define the temperature on the equator of an axisymmetric sphere. Also, thermocouples 11 and 12 can be used to define the temperatures on the top and bottom poles of this axisymmetric sphere. In addition, thermocouple 14 can be defined at a location that is 45 degrees from thermocouple 11 and thermocouple 13 can be defined at a location that is 45 degrees from thermocouple 12 on this axisymmetric sphere. Figure 18 shows the readings of these thermocouples including the TCs average at the equator and Figure 19 shows a diagram of the PBX 9501 axisymmetric sphere including the location of these thermocouples. An Aria C user subroutine was written to define the temperatures at the nodes on the surface of this sphere. These temperatures were defined interpolating linearly assuming that the surface temperature is a function of the angle θ measured from the y axis and shown in Fig. 19. These interpolations were carried out between the thermocouple positions shown in Figure 19. A three dimensional mesh composed of 1413251 tetrahedral elements with four integration points was used to simulate the SITX experiment using the 1D boundary condition estimated previously for $t \leq 20800$ s. In addition, for $t > 20800$ s, the axisymmetric boundary condition defined in Figure 19 was applied on the nodes located on the surface of this 3D mesh. This FE model predicted the thermal ignition time at 49307 s and the experimental time to ignition was 51938 s. This results in a percentage error of -5.1%. This error differs only 1.5% from the error predicted by the 1D solution. Figure 20 compares the FE model response at the center of the sphere with TC 2. Figure 20 shows reasonable agreement between the FE response and the experimental temperature. The location of ignition was predicted at an angle θ of 57 degrees measured from the y axis shown in Fig. 19 and at a radial distance of 1 cm from the surface of the sphere. Figure 21 compares the temperature predicted at the ignition location and TC 6 with thermocouples 6 and 11. An additional

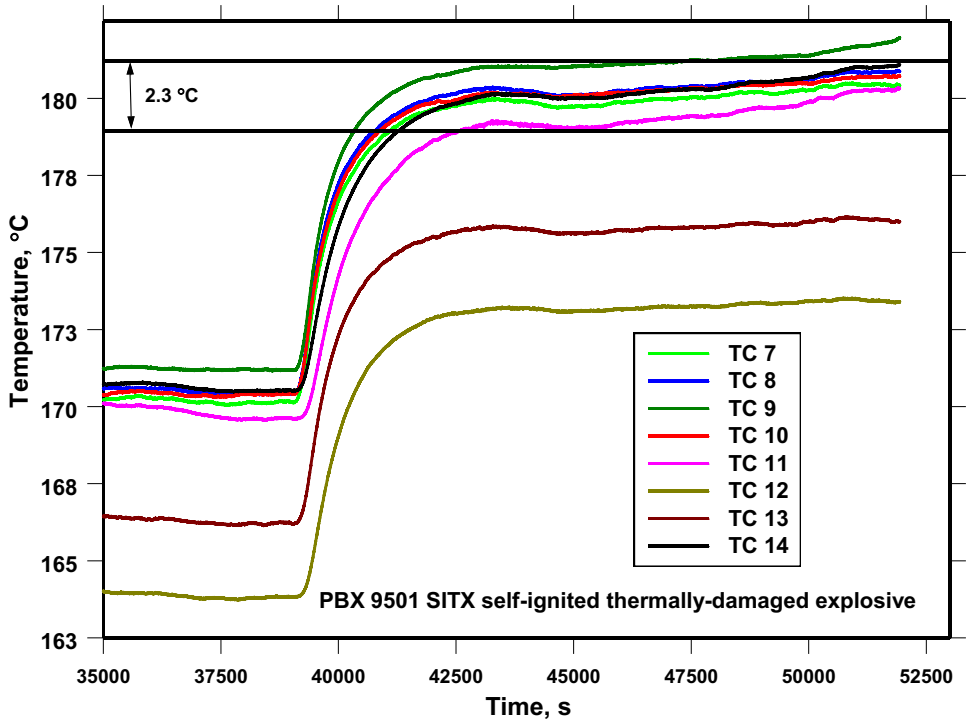

Figure 17. Temperatures measured on the bottom steel bowl and on the surface of the PBX 9501 sphere (see Fig. 4).

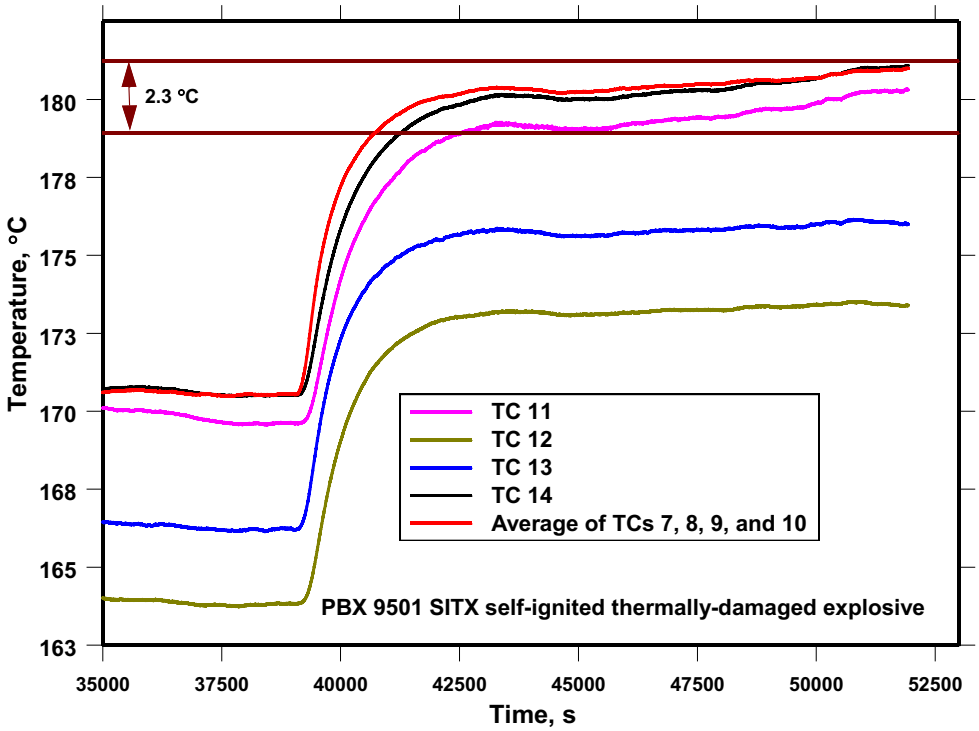

Figure 18. Thermocouples used to define an axisymmetric boundary condition on the surface of the PBX 9501 sphere shown in Figure 19.

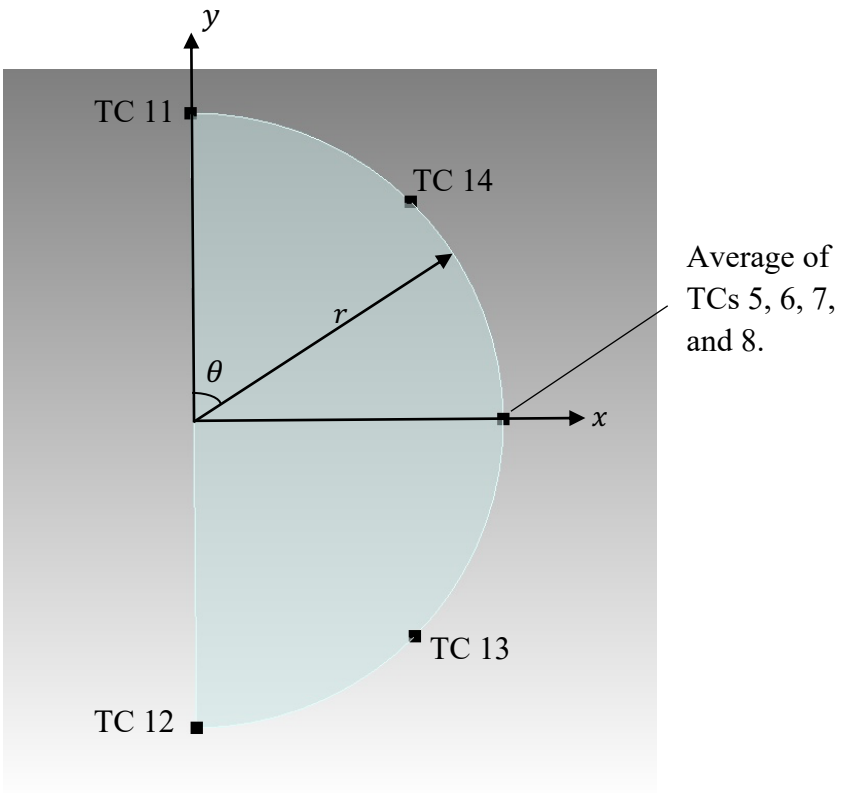

Figure 19. Axisymmetric sphere boundary conditions.

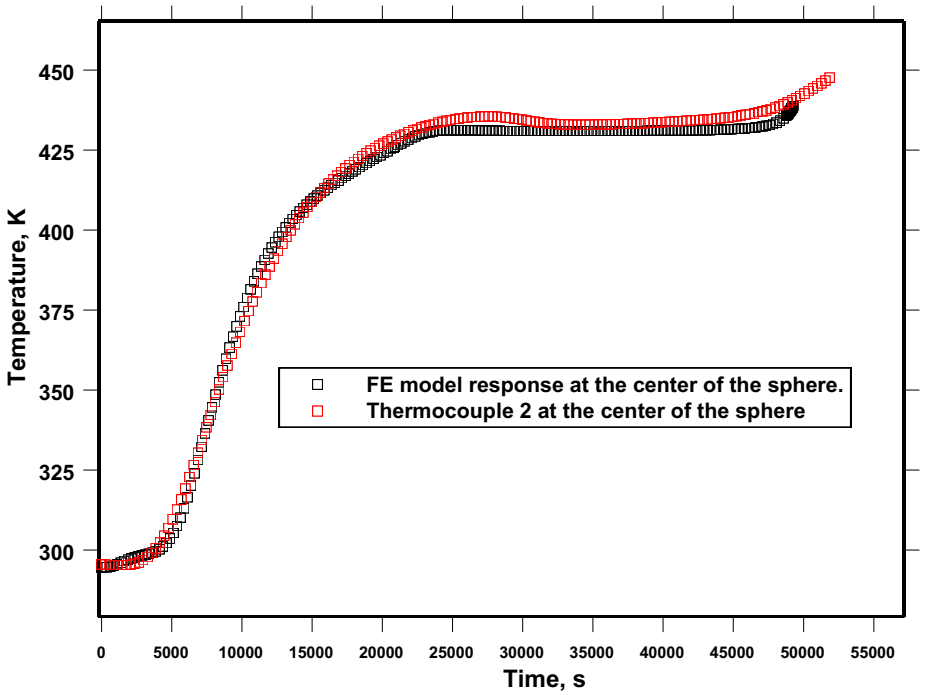

Figure 20. Predicted temperature and thermocouple readings at the center of of the sphere. The 1D boundary condition was applied for $t \leq 20800$ s and the axisymmetric boundary condition was pplied for $t > 20800$ s.

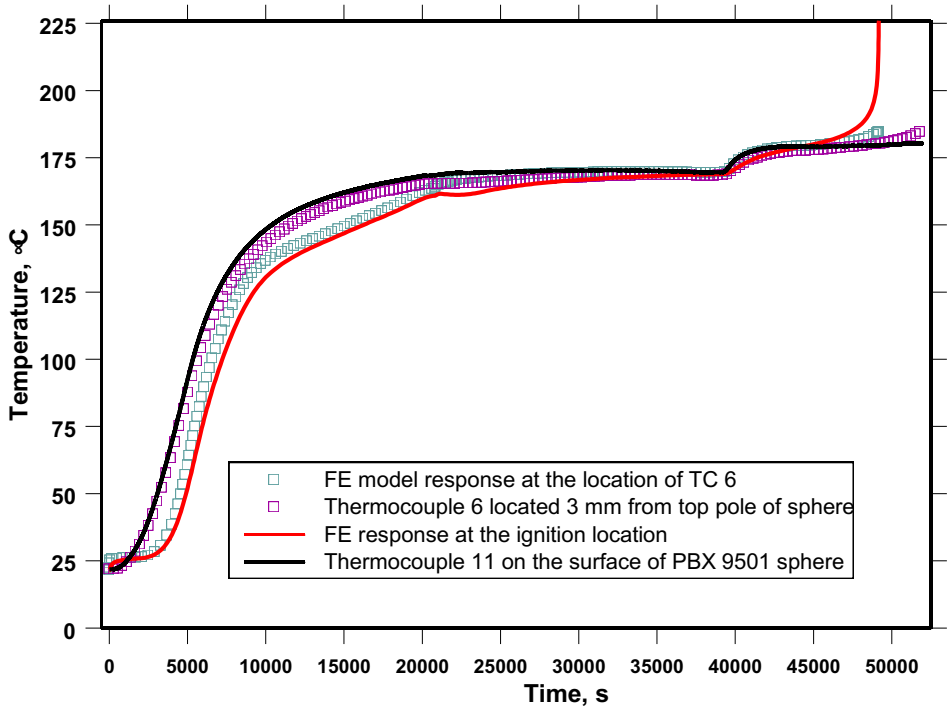

Figure 21. Comparison of the FE response at ignition and at TC6 with TC6 and TC 11. The boundary condition defnied in Fig. 19 was applied.

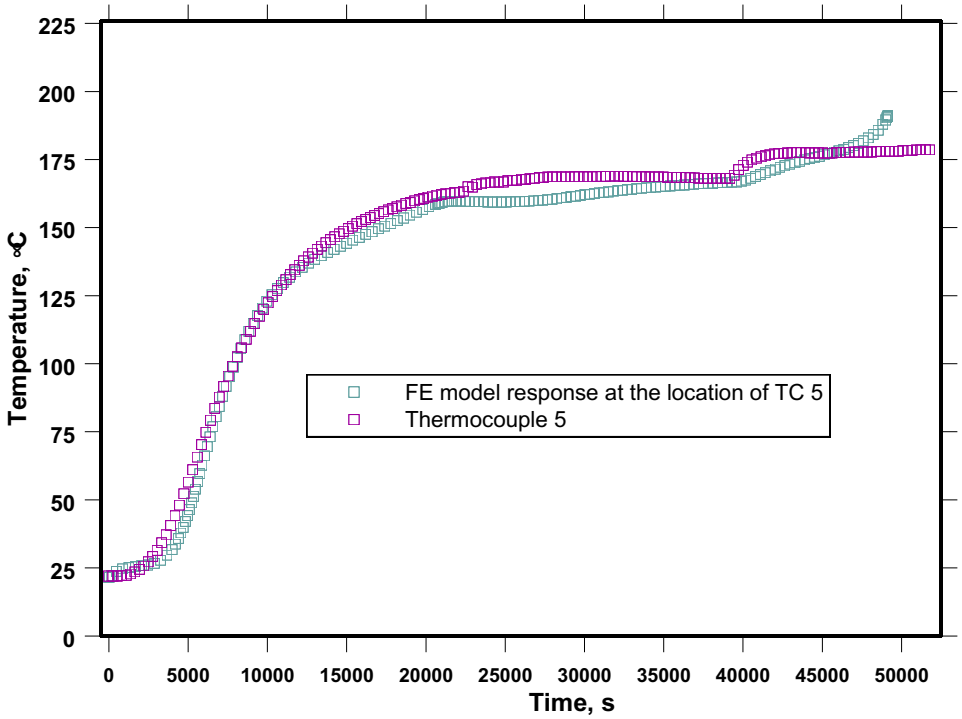

Figure 22. Comparison of the FE response at TC 5 with TC 5. The boundary condition defined in Fig. 19 was applied for this simulation.

comparison of the FE model response at the location of TC 5 with TC 5 is shown in Figure 22. Figure 21 and 22 show reasonable agreement of the FE model with TCs 5, 6, and 11.

Conclusions and Comments

Figure 23 shows the predicted temperature distribution at ignition using the boundary condition defined in Fig. 19. The symmetry shown in Fig. 23 was predicted because of the axisymmetry of the temperature boundary condition. Aria predicted the maximum ignition temperatures at two points that are mirror images of each other. Figure 24 shows the location of these points. Aria predicted a temperature of 550 K at these two points. Figure 23 was obtained passing a vertical plane through the two points shown in Fig. 24. Due to the axisymmetry of the boundary condtion, the predicted hot spot at ignition is a ring with the shape shown in Fig. 23.

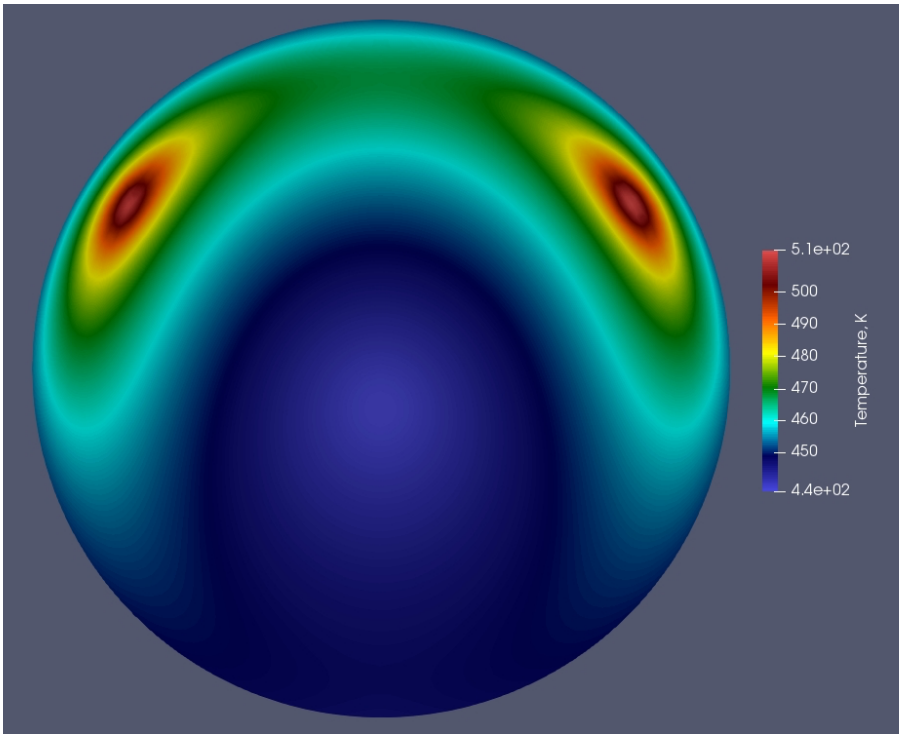

Figure 23. Temperature distribution predicted by the model that used the boundary condition defined in Fig. 19.

The internal temperature measured by TCs 1 to 6 were implemented drilling a blind hole (Figs. 2 and 12) with a diameter of 3.175 mm and potting the thermocouples down the blind hole at different depths. The FE model used to simulate this experiment didn't include the thermal properties associated with the potted bundle of thermocouple wires inserted in this hole. Note from Figs. 21 and 22 that even though the thermal properties of the small cylinder composed of the potting material and the bundle of thermocouples wires that fills the blind hole (Figs. 2 and 12) were not included in the the FE model, the agreements between the readings of TCs 5 and 6, and the FE model responses are reasonable.

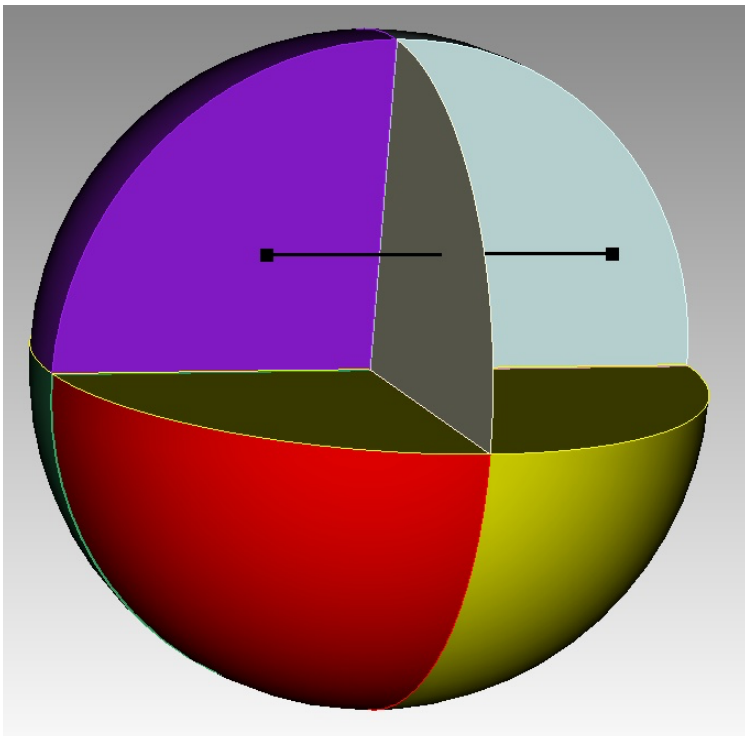

Figure 24. Aria predicted the maximum temperatures at ignition, 500 K, at the two black points shown in this figure.

The temperatures predicted by the 3D axisymmetric model are considered to be more realistic than the 1D solution. Note that for times greater than 20800 s the PBX 9501 sphere was already expanded and this expansion made TCs 7, 8, 9, 10, 12, and 13 (which were taped to the steel) to be in closer thermal contact with the sphere. Table 3 summarizes the 1D and 3D FE solutions obtained in this study.

Table 3. Implemented 1D and 2D FE solutions.

Solution Type	Time to Ignition Error, %
1D for $0 \leq t \leq$ 50072 s	-3.6
1D for $t \leq$ 20800 s, and 3D Axisymmetric for $t >$ 20800 s	-5.1

The SITX experiment resulted in a High Explosive Violent Reaction (HEVR) right after thermal ignition. Reference [1] points out that many indications of Deflagration to Detonation Transition (DDT) were observed for this experiment. Photon Doppler Velocimetry (PDV) was used to probe the dynamic velocity at different locations on the outer surface of the steel vessel. Section 6.2 of reference [1] discusses the velocimetry data associated with DDT for the SITX experiment.

Acknowledgements

The funding provided by Anthony Puckett (R & D Engineer, Q-18) is gratefully acknowledged. I thank the M-6 exprimentalists that contributed to the implementation and execution of the SITX experiment: Matthew D. Holmes, Robert M. Broilo, Ryan C. Rettinger, Andrew T. Barnes, Eric M. Heatwole, Michael A. Englert Erickson, Trevor A. Feagin, Philip J. Rae, Michelle N. Pederson, Peter Dickson, Gary R. Parker Jr. Also, I thank Matt Holmes (M-6) and Gary Parker (M-6) for giving me permission to use some of the figures of reference [1].

References

[1] Holmes, M. D., Broilo, R. M., Rettinger, R. C., Barnes, A. T., Heatwole, E. M., Erickson, M. A. E., Feagin, T. A., Rae, P. J., Pederson, M. N., Dickson, P., Parker, G. R. Jr., "Heavily Confined PBX 9501 Experiment Report FY2020," LA-UR-20-29243, P.O. Box 1663, Los Alamos, NM 87545, 2020.

[2] SIERRA Thermal/Fluid Development Team "SIERRA Multimechanics Module: Aria User Manual – Version 4.58," Sandia Report SAND2020-11537, Sandia National Laboratories, P. O. Box 5800, Albuquerque, New Mexico 87185, Livermore, California 94550, Printed October 20, 2020.

[3] Aviles-Ramos, C. "Two-Dimensional Simulation of PBX 9501 Cook-off Experiments," Los Alamos National Laboratory Report: LA-UR-06-1073, P.O. Box 1663, Los Alamos, NM 87545, 2006.

[4] Dickson, P. M., Henson, B. F., Asay, B. W., and Smilowitz, L. B. "Private Communication," (see Appendix I on page 53 of reference [3]) Los Alamos National Laboratory, P.O. Box 1663, Los Alamos, NM 87545, 2002.